Train Detection by Magnetic Field Measurement with Giant Magnetoresistive Sensors for High-Speed Railway

S. Zhang[1, a], W. K. Lee[2, b], P. W. T. Pong [3,c]

Department of Electrical and Electronic Engineering, The University of Hong Kong, Pokfulam Road, Hong Kong

[a]lakez525@hku.hk, [b]wklee@eee.hku.hk, [c]ppong@eee.hku.hk

Abstract. Train detection, as part of the railway signaling system, is important for safe operation of high-speed railway. The recent flourishing development of high-speed railway stimulates the research need of train detection technology to enhance the safety and reliability of train operation. This paper proposes a new technique for train detection through magnetic field measurement by giant magnetoresistive sensors. This technology was studied by the analysis of magnetic field distribution in the high-speed rail system obtained from modeling and simulation. The results verify the feasibility for detection of train presence, number of rolling stocks, speed, and length. It can overcome the limitations of track circuits and provide additional measurement capabilities to the signaling system. This detection system can be built with low cost and minimal maintenance load as well as compacted construction. Therefore, it may serve as a new train detection system to help improve the current systems, enhancing and promoting the safety and reliability of high-speed rail system.

Introduction

Train detection acquires the occupation status of a rail section. This information is processed by the railway signaling system to exhibit "red" aspect whenever the track segment is occupied. Such mechanism will avoid train collision by ensuring that no more than one train can enter a rail section at the same time.

Track circuits are one of the most commonly used train detection devices. One of the major limitations of track circuits is the requirement for insulated rail joints [1], which induces uncertainties, weakens the mechanical strength of the rail, and has poor compatibility for high-speed rail running on welded rail. The adoption of audio frequency signal in joint-less track circuits can alleviate this problem; however, it increases the cost and maintenance load significantly [2]. Moreover, the fuzzy signal at the border and interference of multiple track-circuit signals need to be carefully handled [3]. Besides, a track circuit encounters problem at grade crossing where multiple tracks cross, creating permanent shunt paths [4]. Several factors such as rust, compacted leaf residue, and wet tunnels may cause abnormal operation of track circuits. Axle counters are also a widely deployed train detection device which counts the number of wheel-pairs passing the detection point at the start of a section. There are several disadvantages for axle counters. In case when the axle counter loses its memory of the axle number, manual reset is necessary to restart the system. This will introduce human factors as a source of unreliability. Second, axle counters cannot work with fail-safe principle. When it works abnormally, the detection of passing wheel-pairs fails and thus the rail section will be marked as unoccupied. Moreover, axel counters have problem when the wheels stop right at the counters. It may also regard the electromagnetic braking devices on high-speed trains as axles by mistake [5]. Apart from the detection mechanisms mentioned above, there are other kinds of detection methods [6] [7]: sense coils detecting the magnetic anomaly caused by the approach of trains; inductive loops between running rails sensing the magnetic field variation due to train motion; trip switch mounted on the overhead lines responding when a train with pantograph passes. These detection techniques can only detect trains in motion; they cannot detect stationary objects. EVA system[6], developed by EVA Signal Corporation, applies infrared beam sensors for stationary train

detection which induces significant expenses. Other detection systems include passive infrared and ultrasonic detections, video imaging, sound detection of locomotive horn, communication-based train detection with on board GPS and wayside radio links [6] [7]. However, they either require expensive equipment and large maintenance load or they are susceptible to interference from various factors such as light condition and temperature of the environment. Therefore, a new detection technique is necessary for high-speed rails which require higher safety standard and more stringent requirement on signaling.

In this paper, a new train detection technique for high-speed rails by magnetic field measurement with giant magnetoresistive sensors is proposed. Magnetic field measurement has been applied in vehicle detection and car speed measurement [8]. Since railway trains contain ferromagnetic materials, it is possible to develop similar method for train detection. The new technique eliminates the need for insulated rail joints, therefore it can work with the welded tracks required in high-speed rail systems. It makes use of the magnetic field generated from the overhead contact systems of high-speed rails and thus it is compatible with all the high-speed rail systems. Moreover, this technique enables continuous detection at grade crossing, requiring no insulated joints or expensive equipment, and it is applicable to both moving and stationary trains. It offers additional features: measure the number of rolling stocks, train speed and length, which may enable us to obtain the train identity. This new technique will be a simple, low-cost, and compact system without the need for a transmitter device or wayside controller. Giant magnetoresistive (GMR) sensors are based on recent developments of thin-film technology which produces films with magnetic-field dependent resistance. The films have a sandwich structure of multiple magnetic and nonmagnetic layers. The resistance reaches its extremes when the layers exhibit anti-parallel or parallel magnetization [9]. Compared to other types of magnetic sensors, GMR sensors have the advantages of low cost, compact-in-size, and low energy consumption.

GMR sensors offer the best performance in terms of cost, size, and energy consumption among various magnetometers such as anisotropic magnetoresistance (AMR) sensors, fluxgate, superconducting quantum interference device (SQUID), and spin resonance [8]. These advantages are beneficial for large-scale application and long-term usage as required for train detection in railways.

In this paper, the feasibility and deployment arrangement of this new technique are analyzed and verified by computational modeling.

Modeling and Simulation

The modeling and simulation were carried out with finite element method in ANSYS Maxwell to solve for static, frequency-domain, and time-varying electromagnetic fields. The entire model is divided into two parts: the electrical circuit for power supply and the train. The circuit consists of overhead contact lines which include a catenary wire and a contact wire, and the return circuit including one negative feeder, one return conductor, two rails, and an earth buried conductor under the ground between the rails. Therefore the circuit is made of five conducting wires and two rails. Figure 1 shows the circuit model. The current flows through the catenary wire and contact wire to supply power for train traction, and returns through negative feeder, return conductor, earth buried conductor and two rails.
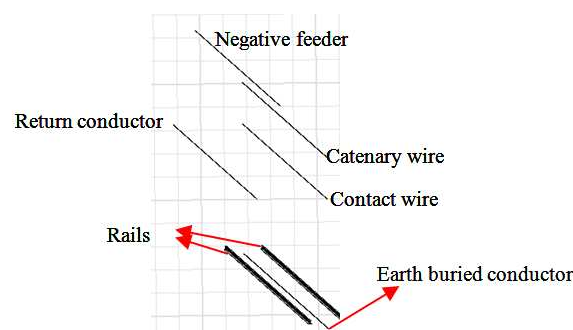

Figure 1. Electrical circuit model for train power supply.

The current values, current types, and conductor materials required for modeling and simulation of the electrical circuit is shown in Table 1. The cross-sections and coordinates for conductors and wires are illustrated in Table 2.

Table 1. Electrical and material details of modeling for overhead contact system

Conductor Name	Current Value [A]	Current type	Material
Catenary wire	+415	Stranded	Copper
Contact wire	+735	Stranded	Copper
Negative feeder	-603	Stranded	Copper
Return conductor	-210	Stranded	Copper
Earth buried conductor	-74	Stranded	Copper
Right Rail	-181.5	Eddy	Stainless steel
Left Rail	-181.5	Eddy	Stainless steel

* The '+' and '-' sign in front of the current value only indicate that two opposite directions for the current in the close loop circuit.
* All currents are 50 Hz AC currents in phase.

Table 2. Cross-sections and coordinates for modeling of overhead contact system

Conductor Name	Cross-section	Radius [m]	Coordinates (x,z) [m]
Catenary wire	●	0.00707	(2, 9.5)
Contact wire	●	0.006	(0, 5.4)
Negative feeder	●	0.006	(0, 7.2)
Return conductor	●	0.006	(3, 5.4)
Earth buried conductor	●	0.006	(0, -0.2)
Left rail			(0.7875, 0)
Right rail			(-0.7875, 0)

* The corresponding points of coordinates are indicated by the dots in the cross-sections.
* The cross-sections for all conductors except rails are approximated by 12-edge polygon with certain radius.

The train model adopted in our simulation is the Deutsche-Bahn ICE 3 high-speed train shown in Figure 2.
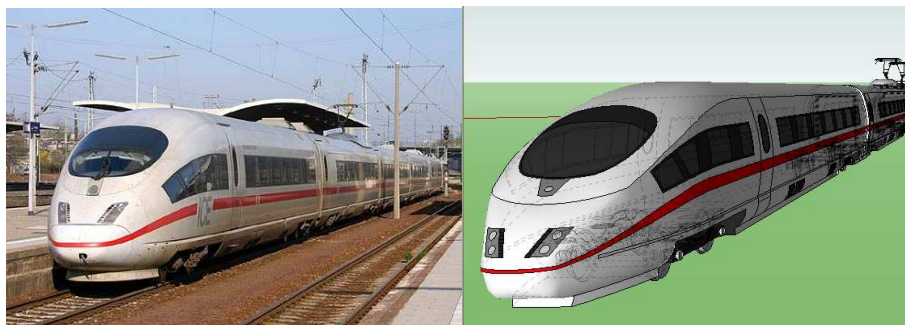

Figure 2. Deutsche-Bahn ICE 3 high-speed train (left)[10] and the structural model of Deutsche-Bahn ICE 3 from google sketchup(right).

The model of the train consists of two heads and six rolling stocks. The material is stainless steel. The train model in different views is shown in Figure 3.

*1. Front view
*2. Top view of entire train
*3. Side view of entire train
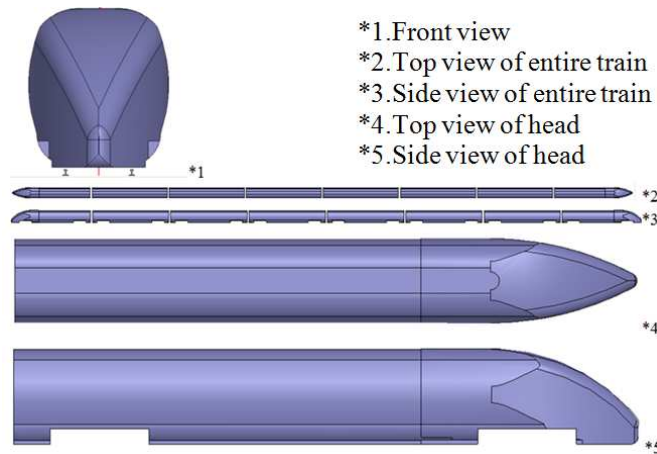*4. Top view of head
*5. Side view of head

Figure.3. Train model in different views.

The entire model is placed along the y-axis (Figure 4). The lengths of all conductors including two rails are 400 m. The length of the train is 196 m. Each head and rolling stock is 7.8 m and 23.8 m respectively. There is a space of 0.6 m between neighboring rolling stocks.
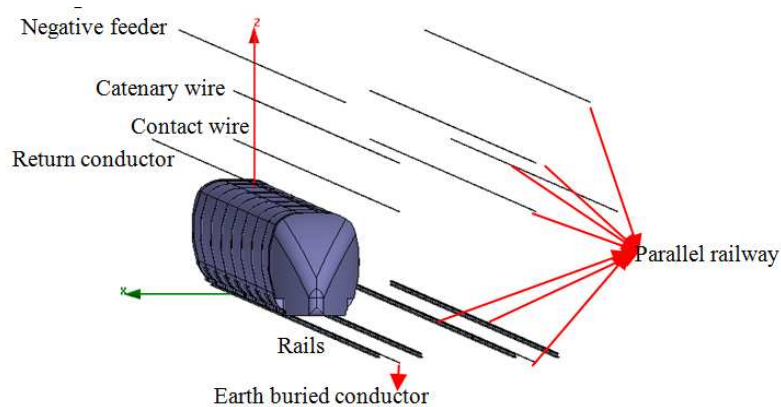

Figure 4. The overall 3D view of the complete model.

To simulate the distribution of magnetic field, all possible sources of magnetic fields within the railway system should be taken into account. Apart from overhead contact systems and other conductors, the sources inside the train must be considered as well. We approximated the sources inside the train with a round copper loop carrying 1000 A, 50 Hz current and simulated its influence to the external field (Figure 5). It can be seen that the generated magnetic field is shielded by the metallic frame of a rolling stock and it cannot penetrate outside the train. Therefore the magnetic field from inside the train can be neglected.
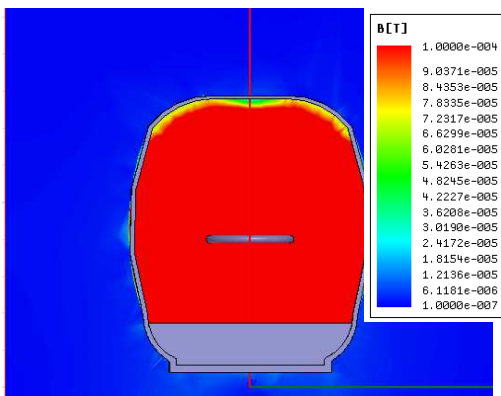

Figure 5. Simulation result of the magnetic source inside the train. A round copper loop with 1000 A, 50 Hz current is put inside the train. The magnetic field generated inside the train ranges from about 20 μT to 100 μT. Since the magnetic field is shielded by the metallic frame, the magnetic field outside the train drops to below 0.1 μT.

The detailed settings for the simulation including solution type, number of adaptive passes, percent error, and refinement per pass are listed in Table 3.

Table 3. Settings and parameters for simulation.

Solution type		Eddy current
Model		3D
Analysis setup	Passes	8
	Percent error	1
	Refinement per pass	30
	Minimum number of passes	2
	Minimum converged passes	1
	Adaptive frequency	50 Hz

Simulation Results and Discussion

Effect of the Train Presence on Magnetic Field Distribution. The simulation result in Figure 6 shows the magnetic field distribution on the XZ plane. The magnetic field is strongest around the wires and conductors, and it decays as it is farther away from these sources. Comparing to the situation without a train (the right half of the simulation), it can be observed that the magnetic field distribution becomes dense and strong above the train, while sparse and weak at the sides of the train. This leads to the phenomenon that the presence of the train warps the magnetic field generated from the wires and conductors—strengthens the field above the train and weakens the field at the sides of the train.
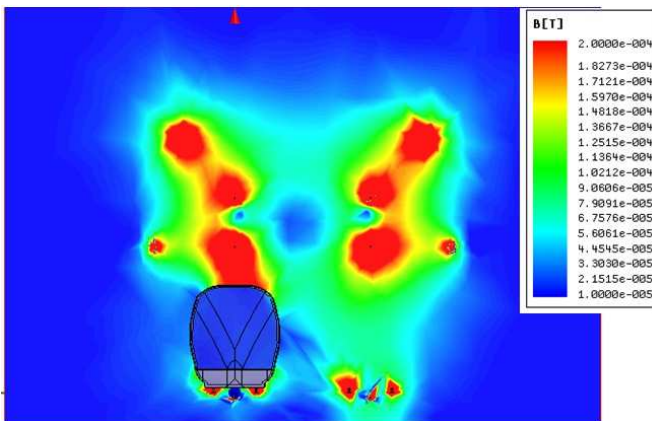

Figure 6. Magnetic field distribution on XZ plane (y = 0). The right half shows the distribution of magnetic field without a train. The comparison between the left and right half shows that the magnetic field above the train is strengthened, while the fields at the two sides of the train are weakened.

Figure 7 shows the effect of train presence on the magnetic field distribution in the top view. The plane selected is right above the train in the XY plane. The outline of the train is overlapped onto the simulation result for better observation. It can be seen that in the area above the train, the magnetic field becomes obviously stronger compared to the regions nearby. At the side of the train, the magnetic field is weakened.
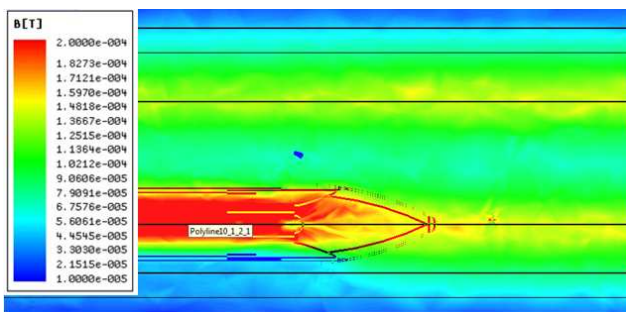

Figure 7. Magnetic field distribution from top view of the model. The chosen plane is in the XY plane (z = 4), i.e. the plane right above the train. The outline of the train is denoted and the lines across the plot are the conductors including catenary wires, return conductors and negative feeders.

According to the simulation results in both Figure 6 and Figure 7, the presence of a train warps the magnetic field generated from the wires and conductors. The effect of the warping above the train is opposite to that at the sides of the train. Above the train, the magnetic field becomes stronger whereas

at the sides of the train, the magnetic field is weakened. Figure 8 and Figure 9 are plots of the magnetic field variation along the rail in the Y direction. The plot starts from one end of the train and extends to 400 m to cover the entire model of the train and the railway system.
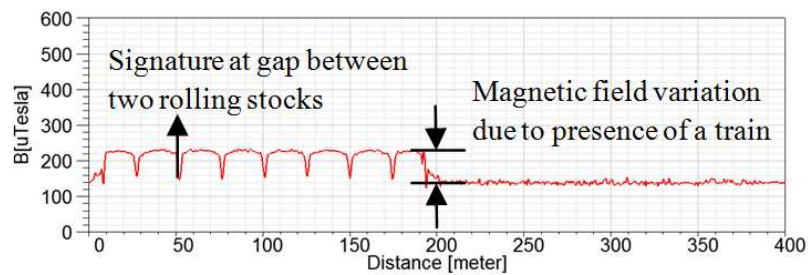

Figure 8. Magnetic field variation along the Y direction (x = 0, z = 4) above the train. The train ranges from 0 to 196 m in the plot.
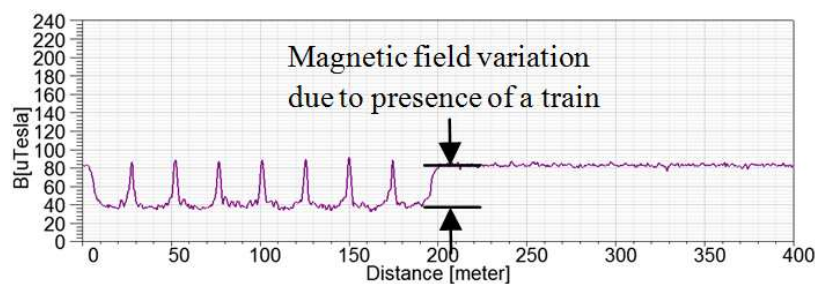

Figure 9. Magnetic field intensity variation along the Y direction (x = 2, z = 4) at side of the train. The line lies in Y direction and passes (2, 0, 4). The train ranges from 0 to 196m in the plot. The arrows denote the sudden changes of magnetic field occurring at the gaps between rolling stocks.

From the magnetic field variation above the train shown in Figure 8, the magnetic field in the region of the train (0 – 196 m) is approximately 80 µT higher than the region without train (196 – 400 m). From the magnetic field variation at the side of the train shown in Figure 9, it can be seen that the magnetic field in the region of the train (0 – 196 m) is approximately 40 µT lower than the region without train (196 – 400 m). An interesting feature worth attention is that there are some pulses in the magnetic field variation. These pulses occur at the gaps between rolling stocks. At these gaps, there are no ferromagnetic materials and thus there are sudden changes in the magnetic field. This signature pattern can be used for counting the number of rolling stocks as explained in Secton 3.4.

From the above results, as a train passes by, the magnetic field will exhibit such patterns of variation and these can provides effective evidence for train presence detection. Since GMR sensors can sense magnetic field from DC to over 1 MHz, stationary trains can also be detected.

Best Positions for Sensors. To determine where to place the magnetic field sensors, there are several criteria. First of all, the sensors must be placed in regions where the magnetic field is warped by the train. Secondly, the magnetic field should exhibit large difference between train presence and no train at that location. The larger the difference, the better the position for putting sensors because of better signal-to-noise ratio.

A few positions were analyzed for their suitability for placing sensors for train detection. The positions were chosen from above the train (A, B, C) and at the sides of the train (D, E, F, G, H, I) as shown in Figure 10. Figures 11 , 12, and 13 illustrate the warping of the magnetic field due to the train along the Y direction from 0 to 400 m at these positions. The positions A, B, and C were chosen to illustrate the difference of the magnetic field variation at different vertical height above the train. The positions D, E, and F were chosen to illustrate the difference of the magnetic field variation at different vertical height at the side of the train. The positions E, G, H, and I were chosen to illustrate the difference of the magnetic field variation at different horizontal distance from the side of the train.
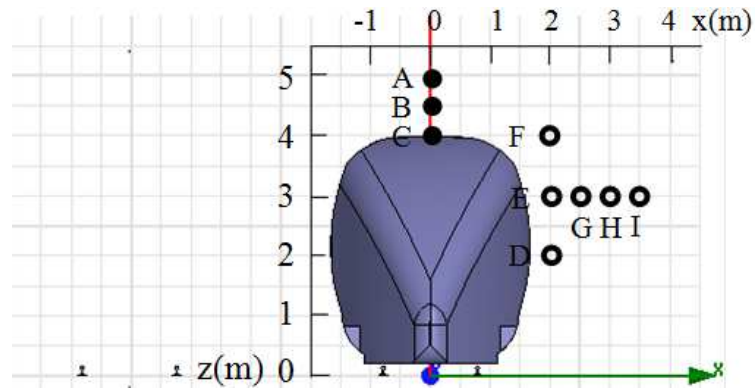
Figure 10. Illustration of the positions selected for investigating the magnetic field variation. Dots are positions above the train and circles are positions at the side of the train. A~I correspond to the plots marked by A~I in Figures 11, 12, and 13.
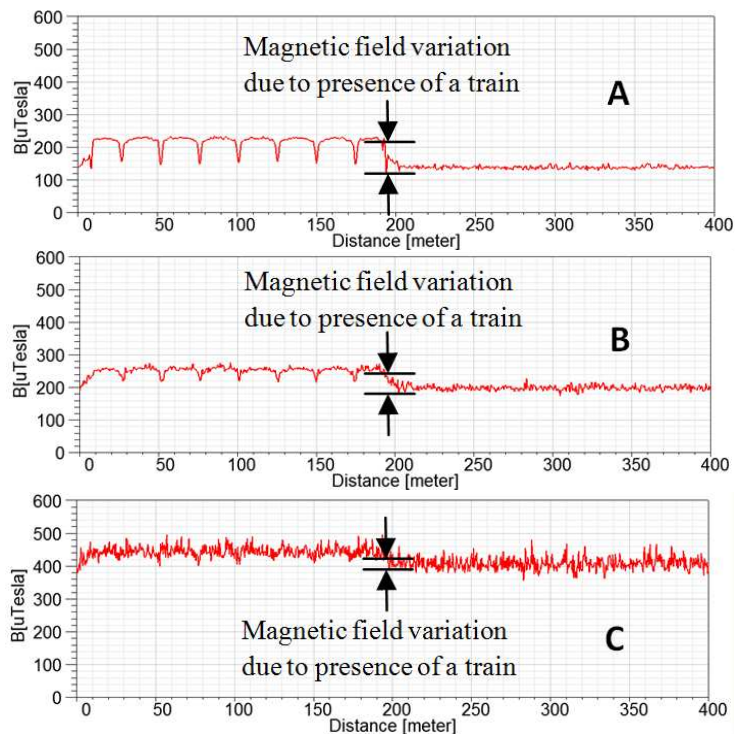

Figure 11. Magnetic field variation above the train at positions A, B, and C: A. along the line passing (0, 0, 4); B. along the line passing (0, 0, 4.5); C. along the line passing (0, 0, 5).

From Figure 11, it can be seen that above the train, the magnetic field variation is different at different height above the train and it is larger for positions closer to the train. As it goes farther from the train in z direction, the variation becomes insignificant.
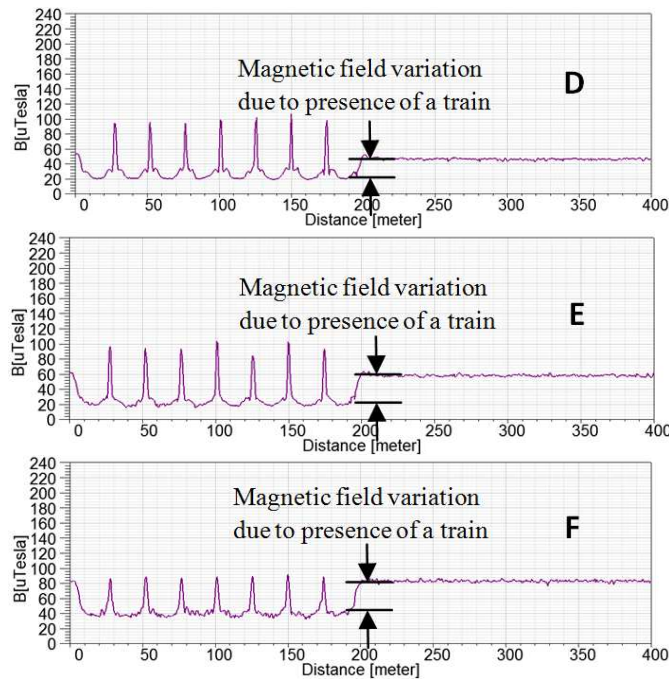
Figure 12. Magnetic field variation at the side of the train at positions D, E, and F: D. along the line passing (2, 0, 2); E. along the line passing (2, 0, 3); F. along the line passing (2, 0, 4).

From Figure 12, it can be seen that at side of the train, the magnetic field variation is larger for positions E and F.
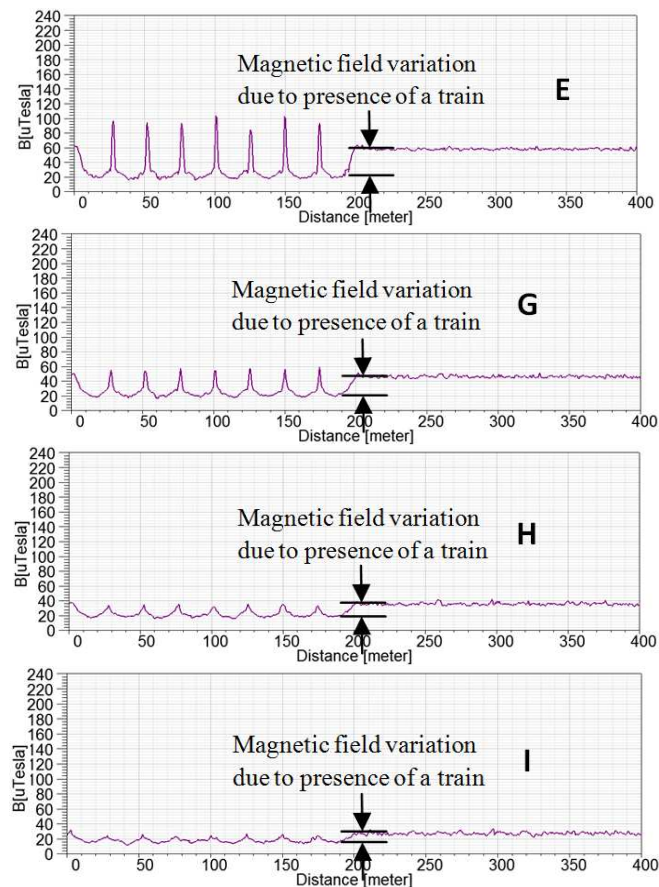

Figure 13. Magnetic field variation at the side of the train at positions E, G, H, and I: E. along the line passing (2, 0, 3); G. along the line passing (2.5, 0, 3); H. along the line passing (3, 0, 3); I. along the line passing (3.5, 0, 3).

From Figure 13, it can be seen that at the side of the train, the magnetic field variation is larger for positions closer to the train. When it is farther away from the train in the x direction, the variation becomes smaller.

According to the above observation and discussion, it can be summarized that: above the train, the warping is stronger at positions closer to the train in Z direction; at the side of the train, the warping is stronger at the vertical levels of z =3 and z=4 than at z=2 and it is stronger at positions with shorter horizontal distance from the train. Therefore, the highlighted regions including positions C, E, and F in Figure 14 are better for placing sensors because the warping of magnetic field is stronger than other regions. These regions can be accessed for placing sensors with a simple structure as shown in Figure 15. Based on the findings in Sections 3.1 and 3.2, the magnetic field measurement can be applied for detection of a set of parameters about the train: presence, number of rolling stocks, speed, and length.
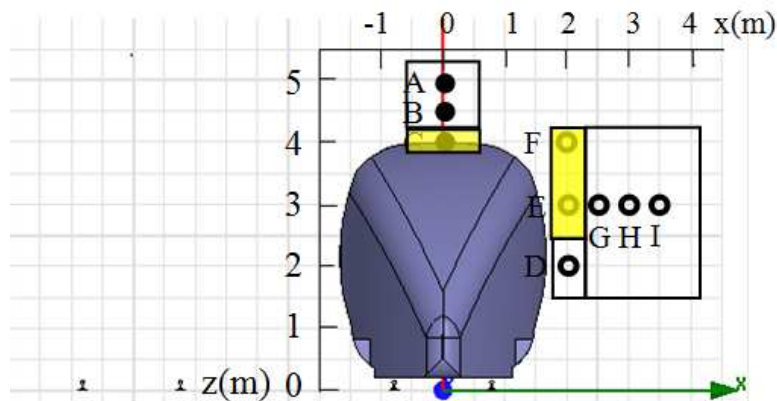

Figure 14. Regions for placing magnetic sensors. The highlighted regions are better places for sensors with stronger warping effect of magnetic field from the train.
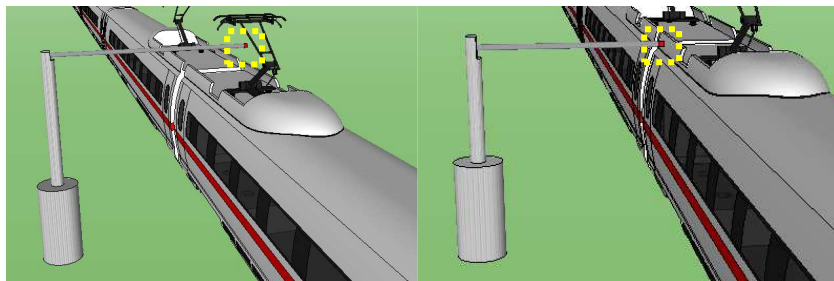

Figure 15. Sensors placed above the train(left) and at side of the train(right). The highlighted component at the end of the bar is the GMR sensor at position enclosed by the dashed box.

Detection of Trains:

Detection of Train Presence. As discussed in Section 3.1, when a train is present, the magnetic field above the train is higher than the case without the train (Figure 8) while the magnetic field is lower at the side of the train compared to the case without the train (Figure 9). Therefore, when a train passes by the sensor or stops next to the sensor, the magnetic field measured will be higher (if the sensor is above the train) or lower (if the sensor is by the side of the train) than the normal level. Therefore the presence of a train can be detected. When the train departs from the sensor, the magnetic field returns to the normal level again.

Detection of Number of Rolling Stocks. In addition to the presence of a train, the magnetic field signatures indicating the gaps between rolling stocks (discussed in Section 3.1) can provide information for counting the number of rolling stocks. Then the number of the rolling stocks is one plus the number of the signatures detected by the sensor during the passing by of the train. If two sensors are placed in the two end of a track section, the number of rolling stocks that enter and leave this section can be recorded and compared to see if the whole train has left the track section.

Detection of Speed. There are two methods for speed detection. With one sensor and known length of each rolling stock, the speed of the train can be deduced. As shown in Figure 16, a train is passing by sensor A which is placed at position E denoted in Figure 10. After the first rolling stock travels past sensor A, the gap between the rolling stocks and thus its signature is detected by sensor A at time t_1. After the second rolling stocks travels past sensor A, and the next gap and its signature occurs at time t_2. If the length of each rolling stocks is given as L and the spacing between two rolling stocks is d. Then the average speed v of the train in this duration is

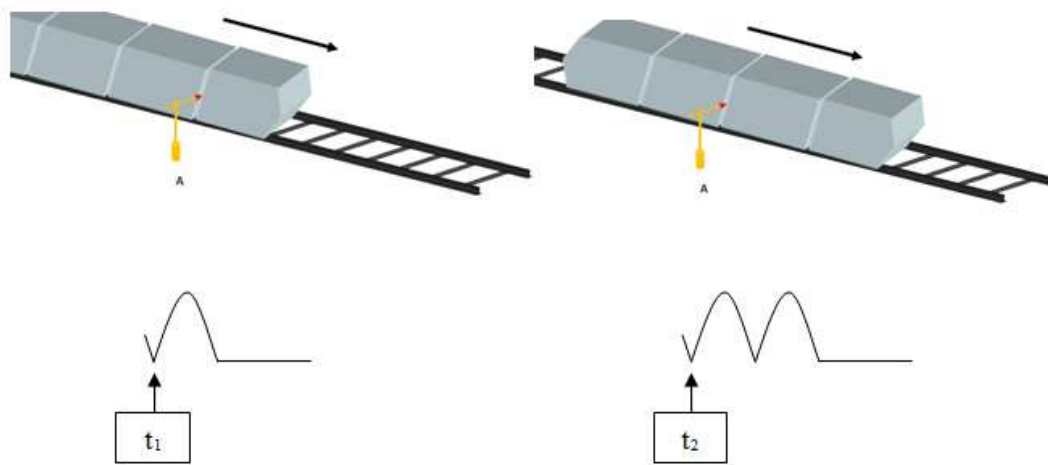$$v = \frac{L + 2(\frac{d}{2})}{t_2 - t_1}.$$

(1)

Figure 16. Illustration for speed measurement with one sensor. A train is passing by sensor A during time $t_1 \sim t_2$. The left diagram shows the situation at time t_1. The right diagram shows the situation at time t_2. The component highlighted in red is the GMR sensor. The arrow indicates the traveling direction of the train. The waveforms below are the corresponding magnetic field variation. It can be seen that the first signature happens at t_1 and the second one occurs at t_2.

The train speed can also be detected with two sensors placing along the rail. In this case, the length of the rolling stock does not need to be pre-determined. As shown in Figure 17, a train is passing by sensors B and C which are both placed at position E denoted in Figure 10. Suppose the occurrence of the first signature is taken as the sign for measuring the speed, sensor B detects its first signature at time t_3, and sensor C detects its first signature at time t_4. The distance L_{BC} between sensors B and C is known, the approximate speed of the train can be obtained as:

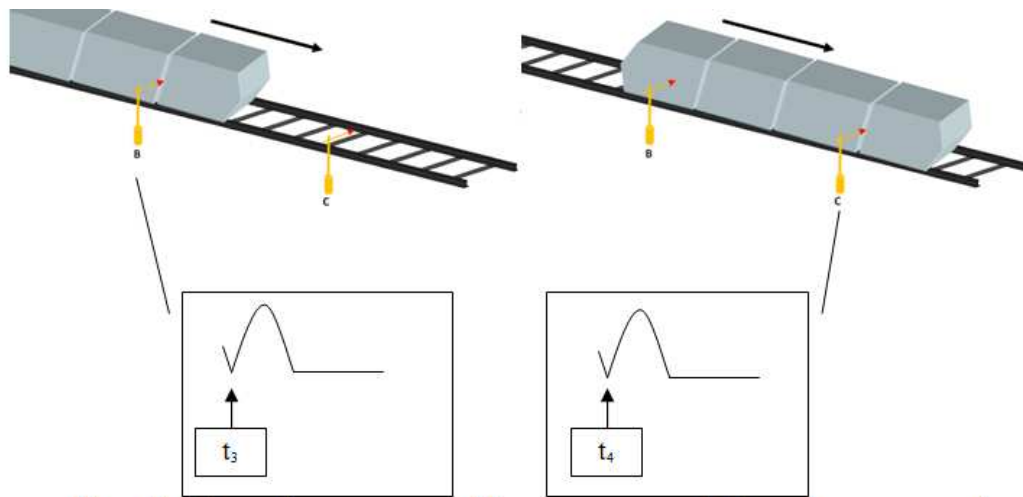$$v = \frac{L_{BC}}{t_4 - t_3}.$$

(2)

Figure 17. Illustration for speed measurement with two sensors. A train is passing sensor B and sensor C during time $t_3 \sim t_4$. The left diagram shows the situation at time t_3. The right diagram shows the situation at time t_4. The components highlighted in red are the GMR sensors. The arrow indicates the traveling direction of the train. The waveforms below are the corresponding magnetic field variation. It can be seen that at t_3, sensor B has its first signature; while at t_4, sensor C has its first signature.

Detection of Length. If the train speed is known, the length of the train can be derived by measuring how long it takes for the entire train to travel past the sensor. As shown in Figure 18, a train is passing by sensor D which is placed at position E. The head of the train passes the sensor at time t_5 while the tail passes the sensor at time t_6. The sensor D will detect the magnetic field variation due to the train presence starting from time t_5 until t_6 when the train has left. If the speed of the train is v, the length of the train l will be

$$l = v(t_6 - t_5).$$

(3)
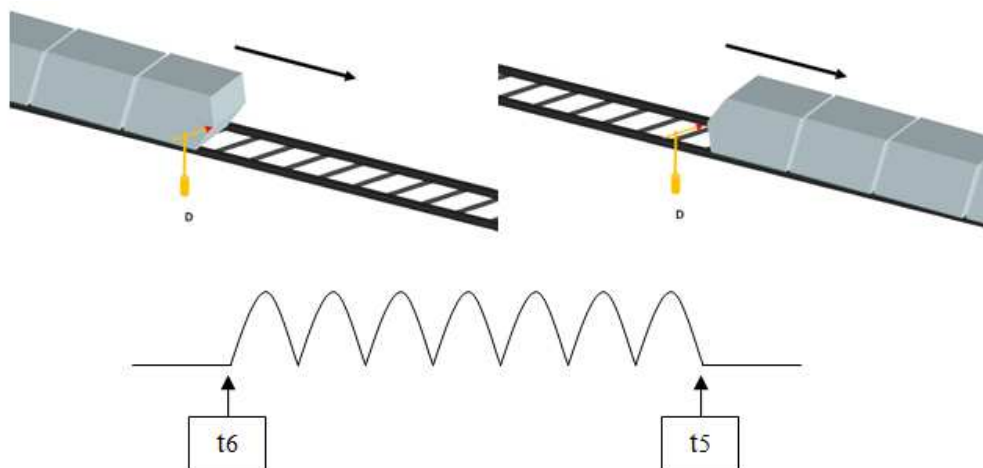
Figure.18. Illustration for train length measurement with one sensor. A train is passing sensor D during time $t_5 \sim t_6$. The left diagram shows the situation at time t_5. The right diagram shows the situation at time t_6. The arrow indicates the traveling direction of the train. The waveforms below are the corresponding magnetic field variation. It can be seen that the variation starts at t_5 and ends at t_6. This means that the entire train passes during $t_5 \sim t_6$.

Fail-Safe Mechanism. Fail-safe principle requires that if the detecting device is broken or fails to work, the signal will indicate the track section as "occupied" therefore no trains can enter. By defining proper corresponding logic values for the magnetic field levels, our technique can be fail-safe. This can be realized when the sensor is placed at the side of the train, rather than above the train. Taking the magnetic field variation at position E as illustration, the red line at level $40^{\mu T}$ is taken as the reference line (Figure 19). The comparator defines the magnetic field above this reference line as logic "1", and that below as logic "0". When there is no train and the sensor works well, the magnetic field measured is above the reference line and thus the comparator outputs "1" which indicates a proceed signal. In the presence of a train, the magnetic field drops to the lower level and the comparator outputs "0" which indicates a stop signal. If the sensor fails, there is no magnetic field detected and the comparator will keep providing a logical output of 0 indicating a stop signal.
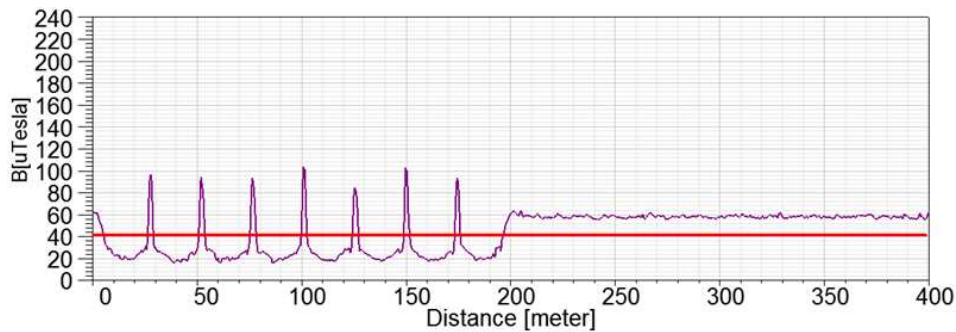

Figure 19. The mapping of analog value of magnetic field intensity to logic '1' and '0'. The red line at $40^{\mu T}$ is chosen to be the reference line. The value above the baseline is logic '1', below is logic '0'.

Defining variable a as the presence status of a train ("0" = no train, "1" = train presence), and variable b as the working status of the sensor ("0" = fail, "1" = working), and the logical output of the comparator is s ("0" = occupied, "1" = un-occupied). Then according to the above description, the relation of a, b and s is given by Eq.4 and the logic table is shown in Table 4.

$$s = \bar{a} * b .$$ (4)

Table 4. The logic table for different cases of train presence and sensor working status. 'a', 'b' and 's' are the presence status of a train, the working status of the sensor, and the logic output of the comparator respectively.

Cases	a	b	s	Signal
No train & device works	0	1	1	Proceed
With train & device works	1	1	0	Stop
No train & device fails	0	0	0	Stop
With train & device fails	1	0	0	Stop

It can be seen that the detection system will produce a logic '1', i.e. a "proceed" aspect signal only in the case when there is no train and the device works normally. The signal will be "stop" for all other cases including the cases when the sensor fails. This meets the fail-safe principle.

Advantages. The new technique for train detection overcomes some of the shortcomings of track circuits. Firstly, since the detection only depends on the information of magnetic field distribution in high-speed rail system, it has no need for special features of tracks, such as insulated rail joints; secondly, the detection is based on the warping effect on magnetic field by a train, which does not lose effectiveness at grade crossing; moreover, the detection is immune to factors such as rust and wet environment because these have no influence on the magnetic field.

The new technique also has advantages in cost, size, and energy consumption. The major components for detection, GMR sensors, cost just a few US dollars each. A GMR sensor is only a few mm in size which leaves plenty of margin for construction space. The power consumption for each sensor is only around 10 mW and thus a battery can last for long time without maintenance [11].

The new train detection system has relatively low complexity because its realization does not require transmitter devices or wayside controllers. Moreover, unlike some of the train detection methods which require additional processing of the raw detection data, for example, the image video detection technique requires post-processing of images, the GMR sensor converts the magnetic field measurement into electrical signal directly. Thus this eliminates the need for more complex equipment or additional data processing.

References

[1] A P Patra and U Kumar, Availability analysis of railway track circuit , Institution of Mechanical Engineers. Proceedings. Part F: Journal of Rail and Rapid Transit. 224. 2010. pp. 169-177.

[2] N. Nikolov and N. Nedelchev , Study on centre-fed boundless track circuits. IEE Proc.-Electr. Power Appl., Vol. 152, No. 5, September 2005

[3] AKIO TAGUTI , Improvement of border characteristics of jointless track circuit. Electrical Engineering in Japan, Vol. 127, No. 4, 1999

[4] Patent_train detection system for railroad grade crossing. United States Patent. Apr. 2, 1973.

[5] United States Patent, Method of detecting obstacles on railroad lines, Patent No. US 6,565,046 B2. May 20, 2003.

[6] U.S. Department of transportation, Federal Railroad Administration. Evaluation of alternative detection technologies for trains and highway vehicles at highway rail intersections, February 2003.

[7] Transportation Research Board, National Research Council. Traffic signal operations near highway-rail grade crossings, 1999.

[8] J. Pelegri, J. Alberola, V. Llario, Vehicle detection and car speed monitoring system using GMR magnetic sensors, IEEE. vol.2, 2002, pp. 1693 - 1695.

[9] Robert W. Schneider, Carl H. Smith, Low Magnetic Field Sensing with GMR Sensors Part 1: The Theory of Solid-State Magnetic Sensing, September 1, 1999.

[10] Information on http://www.railway-technology.com/features/feature1533/feature1533-4.html

[11] Information on http://www.nve.com/Downloads/analog_catalog.pdf